2020 USGS NEHRP Final Technical Report

Investigating the Earthquake Chronology of the Last Millennium along the Cholame Section of the San Andreas Fault: Collaborative Research with Arizona State University and San Diego State University

Researchers
J Ramón Arrowsmith (Principal Investigator) & Alana Williams
Ramon.arrowsmith@asu.edu
Alana.M.Williams@asu.edu
School of Earth and Space Exploration Arizona State University
Tempe, AZ 85287
480-965-3541 office
480-965-8102 fax

Thomas Rockwell
trockwell@sdsu.edu
San Diego State University
5500 Campanile Dr.
San Diego, CA 92182-1020
619-594-4441 office
619-594-4372 fax

March 2019 through February 2020

Acknowledgment of Support: This material is based upon work supported by the U.S. Geological Survey under Grant No. G19AP00032 & G19AP00031

Abstract

The Cholame section of the San Andreas Fault (SAF) is located between the partially creeping Parkfield section and the locked Carrizo section. This portion of the fault is significant because it marks a behavioral transition between Parkfield in the north with its creep and numerous M6 earthquakes, and Carrizo in the south with its century-long recurrence intervals. Although offset reconstructions exist for this ~75 km reach, rupture behavior is poorly characterized, limiting seismic hazard evaluation.

We present paleoseismic results from 4 fault perpendicular trenches at the new site named Miller's Well and 2 fault perpendicular trenches from LY4 (previously studied by Arrowsmith and colleagues). The Miller's Well site is 3 km northwest of Highway 58 next to Twisselman Mine. Site geomorphology is characterized by a southwestward draining alluvial fan ~50m wide depositing against a ~10 m high northeast-facing SAF- bounded scarp. We collected ^{14}C five dates to determine the approximate age of the most recent earthquake (MRE) and penultimate event and logged stratigraphy, however the ages were too old to be for the MRE, indicating heavy bioturbation and lack of continuous sedimentation; 1332 ± 70 cal BP, 983 ± 60 cal BP, 941 ± 50 cal AD, and 1005 ± 30 cal AD. Miller's Well turned out to be a poor paleoseismic site because of a lack of preserved and distinctive sediment markers and apparently low prehistorical sedimentation rates, however it provided interesting data for studying the geomorphic features and fault geometry near the transition from the Cholame section to the Carrizo section.

We opened two new trenches at the LY4 paleoseismic site located 10 km northwest of Miller's Well. Geomorphology at LY4 is characterized by alluvial fans depositing across the SAF between linear scarps northwest and southeast of the trench locations. We found evidence for 5-7 ground rupturing events including the MRE in 1857, compared with the 3-4 events previously cited in Stone et al., and Young et al., 2002 for the same stratigraphic sequence. Of these events (labeled as E1-E7) E1, E2, E4, E5, and E6 have high quality evidence. Radiocarbon dates for these ruptures are currently pending.

Introduction and Background

The Cholame section of the San Andreas Fault (SAF) is approximately 75 km long, extending from Highway 58 to Highway 46, northwest of the locked Carrizo section and southeast of the Parkfield section with its mix of M6 earthquakes and creep (Figure 1). The timing of rupture events along the Cholame section is not well known, leaving the details of when and how the slip deficit is released unresolved and how ruptures occur along this important transitional section of the southern SAF uncertain. The large distance spanning the Cholame section and bounding sites provides adequate space for an M6-7 rupture to go unrecorded at the previously studied sites. Current rupture models for the Cholame section are constrained locally only by limited paleo-earthquake offset and timing information, the regional millennial scale SAF slip rate, and the behavior of the adjacent sections (Parkfield and Carrizo; Field, et al., 2013). Present data suggest several rupture possibilities: (1) independent M6-7 rupture of the separate sections (Parkfield, Cholame, & Carrizo) with possible continuation into neighboring sections, (2) reactivation of the 1857 reach (M7.8; possibly involving, triggered by or anticipated by Parkfield M6 events; Sieh, 1978a,b; Toke and Arrowsmith, 2006), and/or (3) aseismic creep (Young et al., 2002). The current Cholame paleoearthquake record is insufficient for any maximum likelihood recurrence interval estimation, which we have begun to rectify with this research and previous trenching completed by this group.

Assuming Cholame should slip at the SAF long term slip rate (~33mm/yr), and the 1857 rupture produced slip of at least 3 m (Sieh, 1978a; Sieh and Jahns, 1984; Young, et al., 2002; Lienkaemper, 2001; Zielke, et al., 2010; 2012), there is a large slip deficit that could be accommodated by a M7 rupture along the full length of the Cholame section (Toke & Arrowsmith 2006). While no significant surface slip has been reported along the Cholame section since 1857, subsequent Parkfield events and creep have terminated around Highway 46 (the northwest end of Cholame section), and Young et al. (2002) report possible post 1857 surface cracking at LY4.

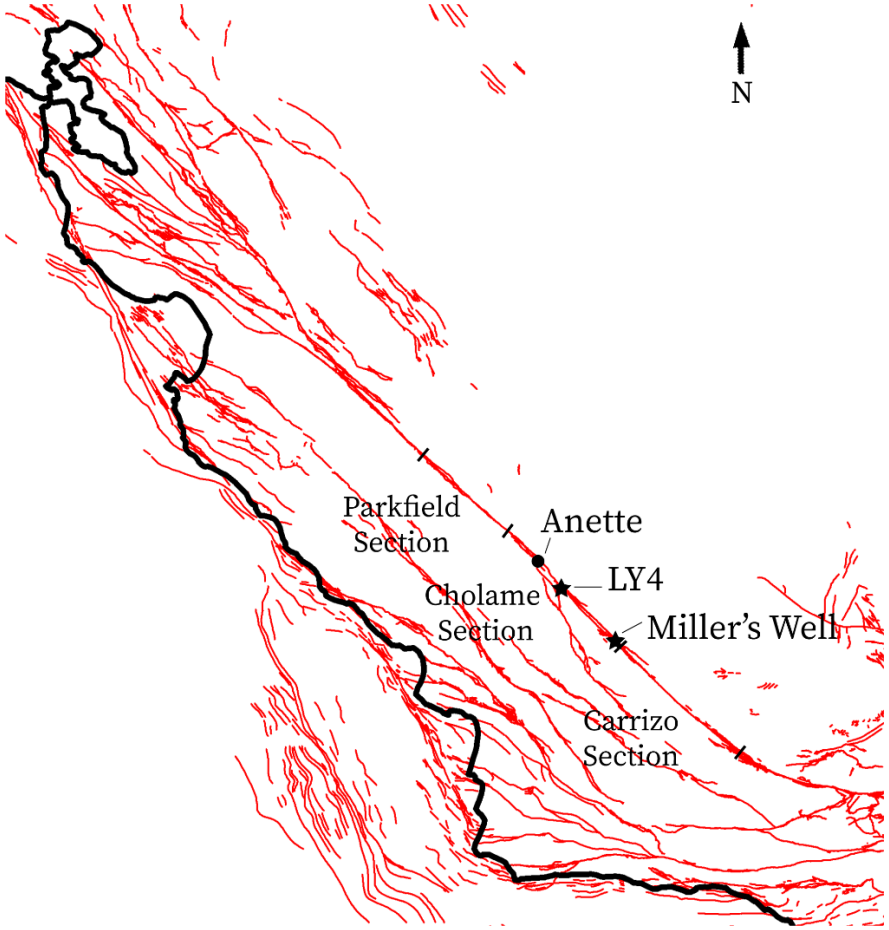

Figure 1. Locations of relevant paleoseismic sites on the Cholame section of the San Andreas fault with Quaternary active faults (USGS Quaternary Fault and Fold Database) shown in red. LY4 and Miller's Well are the focus of this report.

Young et al.'s subsurface measurement of 3.0±0.7 m slip in the 1857 earthquake at LY4 along the Cholame section is smaller than the offsets measured on the neighboring Carrizo section, and much larger than the neighboring Parkfield section, which suggests differences in fault properties (Sieh, 1978a; Hilley, et al., 2001). Young et al. (2002) interpreted 3 ground-rupturing events, one of which was the 1857 event, followed by possible surface cracking. This corresponds with Stone et al.'s (2002) interpretation of 2-4 ground rupturing events since the 12th century and provided a recurrence interval of 290-410 years. This longer recurrence rate differs from a hypothesis of more frequent earthquake recurrence on the Cholame fault section (Sieh and Jahns, 1984; Young et al., 2002) derived from an assumed smaller slip/event in Cholame than Carrizo in 1857, and uniform long-term slip rate along strike. The ages of the past events noted by Young, et al. (2002) and Stone, et al. (2002) were poorly constrained at Cholame due to a lack of datable material.

Previous results from the Annette Paleoseismic Site (18 km northwest of the LY4 site) developed evidence for 6 ground ruptures in the last 900 years and one ground cracking event post-1857 (Williams et al., in prep, Williams et al., 2016). The historic-era ground cracking is consistent with a ground shaking event reported at LY4 and farther southeast in the Carrizo Plain. Of the 6 paleoearthquakes at Annette, four are of excellent quality and two are lower quality and less certain. We have quantitatively rated these events for correlation with other paleoseismic sites to improve the hazard models for the southern San Andreas fault, following the ranking system outlined in Scharer et al., 2014.

Paleoseismic studies southeast of the Carrizo section at Frasier Mountain present evidence for 6 or 7 earthquakes (Figure 2) within the past 650 years, indicating a 90-110-year recurrence interval (Scharer et al., 2014 and 2017). This is consistent with the Bidart record from the Carrizo Plain, which implies a surface rupture recurrence of 88±41 years (Akciz et al., 2010). Chronologic correlation of the Annette record with Bidart events suggest that 4 of the 6 events are associated with Carrizo surface ruptures. The 6-event record at Annette does not appear to be consistent with slip-predictable behavior, however the chronology is not refined enough to say for certain and we hope to resolve this question with the new trenches excavated at LY4.

Previous excavations along the Cholame section by our group have found adequate stratigraphy but a dearth of carbon. Choosing sites is further complicated by the complex fault geometry and the geomorphology of the Cholame section, which can be divided into three distinct sections. The central portion is defined by Cholame Creek, which has deeply incised along and parallel to the fault trace. The southeastern section, where Miller's Well is located, marks a transition from the Carrizo simple fault trace geometry to a wider shear zone. There the fault zone varies in width from several meters to more than 1 km and is expressed by en echelon overlapping sub parallel tectonic landforms.

The faults have been mapped in this region by others using two main approaches: classic field mapping with topographic maps and aerial photography and mapping using lidar-derived topography (Vedder and Wallace, 1970, Stone et al., 2001, Arrowsmith and Zielke, 2009, Lienkaemper et al., 2014). Based on our recent difficulties locating the SAF trace at Miller's Well, these maps are worth reevaluating. Neither method placed the main active trace in the correct location, although the lidar does pick up a small trough as a possible secondary fault. Near Miller's Well, the fault appears to split into two main traces ~ 20 km northwest and ~5 km southeast of this site, unlike the main fault trace at LY4, which seems to be much simpler. This mapping is essential in searching for suitable paleoseismic sites in addition to field inspection.

In this report, we summarize our USGS-supported work in 2019-2020 along the Cholame section. We worked at two places: Miller's Well and LY4. Both are on private property and we are grateful to the landowners (Twisselman Family and Joe Sill) for their permission to work there.

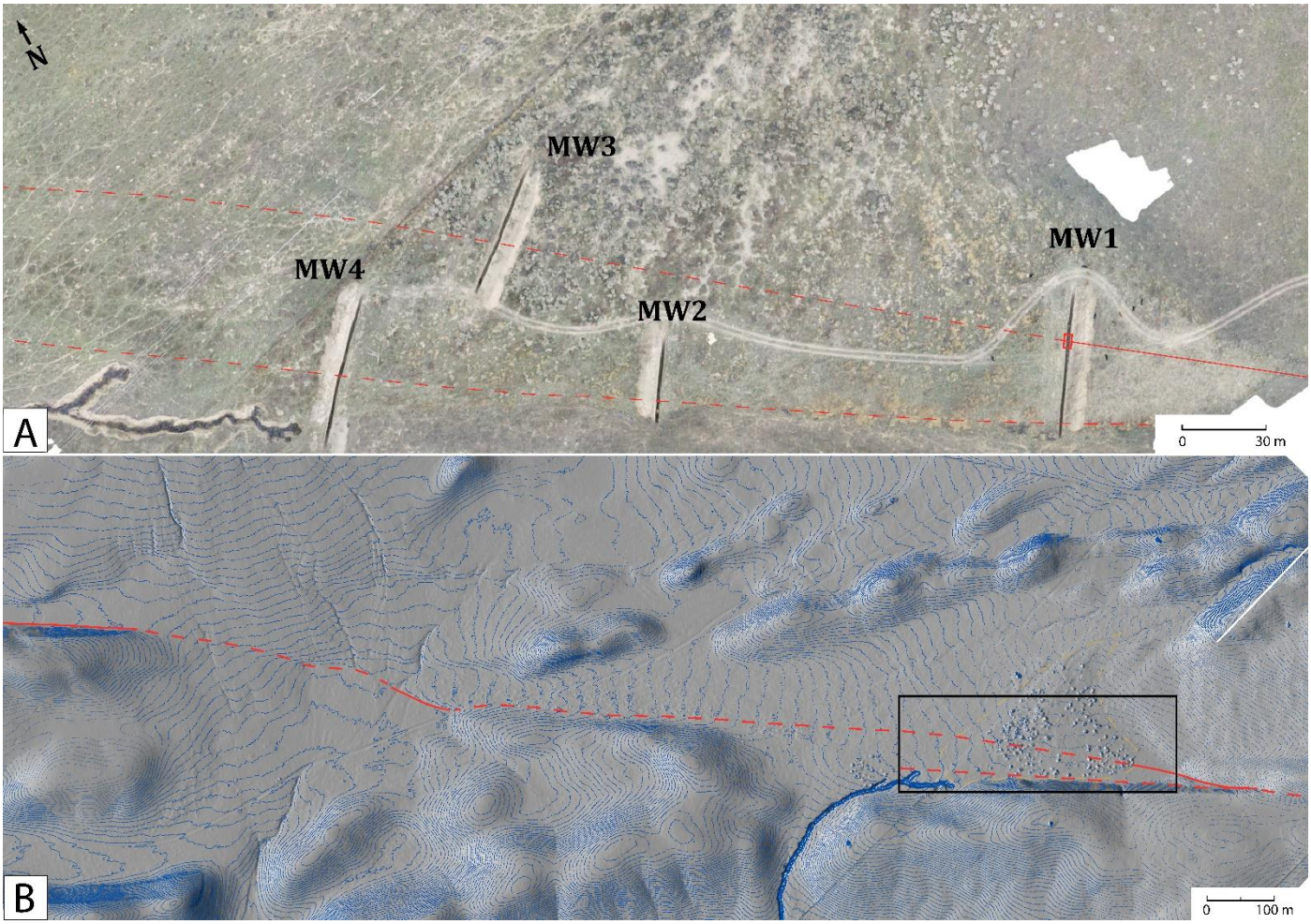

Figure 2. Maps of Miller's Well Paleoseismic site along SAF Cholame section. A) High resolution Structure from Motion orthophoto of the trenches at Miller's Well derived from UAS aerial photography. Faults are displayed in red. Red box on MW1 indicates the location of the trench log in Figure 3. B) B4 lidar hillshade showing the location of the Miller's Well trenches with 0.5 m contour lines in blue, modern fan outlined in yellow, and faults in red. Inset box displaying the structure from motion orthophoto extent.

Miller's Well

Site geomorphology

The Miller's Well site is located on an approximately 50 m-wide alluvial fan. The fan is bounded on the southwest side by a northeast-facing 10 m high scarp and in the north by small en echelon ridges (Figure 2). There is a small channel on the northeast side of the fan that trends oblique to the SAF before turning parallel northwest of our trench locations. A deeply incised channel cuts west between the two shutter ridges, with the knickpoint just beyond the end of MW3. The fan appears to be filling in a depression against the scarp and in between the shutter ridge.

Site Excavations

We initially excavated two trenches "MW1" and "MW2" (Figure 2) but were unable to find the fault zone. The stratigraphy was poor near the hillside where we thought the fault was located. We dug "MW3" where we projected the fault trace would be in the fan, but we found only young sediments down to ten feet. We suspect that the modern fan filled in an erosional depression along the northern end of the scarp (Figure 5) which carved a similar path to the modern channel seen in the aerial orthophoto. After discussion of fault zone location, we decided to extend MW1 and found the trace 20 m away from the end of the initial trench. Following the new projection, we decided to try and find the fault trace in the fan once more and dug MW4. We did not, however, encounter the fault zone in MW4.

Results

The stratigraphic layering in MW1 is heavily bioturbated and mixed, resulting in relatively homogenous strata. The fault zone consisted of an eastern splay with apparent reverse slip and a capping sag that may indicate warping. The main fault zone displayed interpretable stratigraphy on only the northeast side, with massive soil and rare sandy blocks on the southwest (Figure 3). The lack of lateral continuity and the incomparable sediment packages on each side of the fault zone in MW1 suggested two options: either the sedimentation rate was greater than we anticipated and the corresponding stratigraphy was buried deeper, or some units had not been preserved. The ages we received for four samples collected were, 1332 ± 70 cal BP, 983 ± 60 cal BP, 941 ± 50 cal AD, and 1005 ± 30 cal AD, indicating that sedimentation is insufficient for a complete earthquake event record. (Table 1). Sample location with relation to the fault zone can be seen in Figure 3.

MW3 and MW4 both displayed young fan material to a depth of 3-4 m (Figure 4) indicating that the fault trace was buried much deeper than expected. The stratified alluvial fan material is continuous and undisrupted by bioturbation, which is consistent with very active fan and rapid, historical deposition. The ground surface and lidar-derived dems displayed a higher density of shrubbery on this portion of the fan which supports this idea. However, the change in thickness of the modern fan material from MW1 and MW2 to MW3 and MW4 is drastic compared to the topographic surface expression across the fan. An explanation for this is vertical erosion to create a depression which is then filled by fan material, followed by periods of lateral erosion of the shutter ridge (Figure 5).

Because the age of the sediments was mostly too young (MW2, MW3, and MW4) and the stratigraphy too low quality (MW1), we decided to abandon Miller's Well and move to LY4. Nevertheless, these trenches provide us with an unusual opportunity to review the previously published Quaternary fault mapping for Cholame. The sections of the SAF in this region have been broadly defined by the fault geometry and complexity of the fault traces. If the surface mapping is incorrect we can reevaluate the validity of the section distinctions and their implications for hazard modeling. Furthermore, we can use this data to look at the geometry of the fault trace in this region and the paleogeomorphology as it relates to locating good paleoseismic sites.

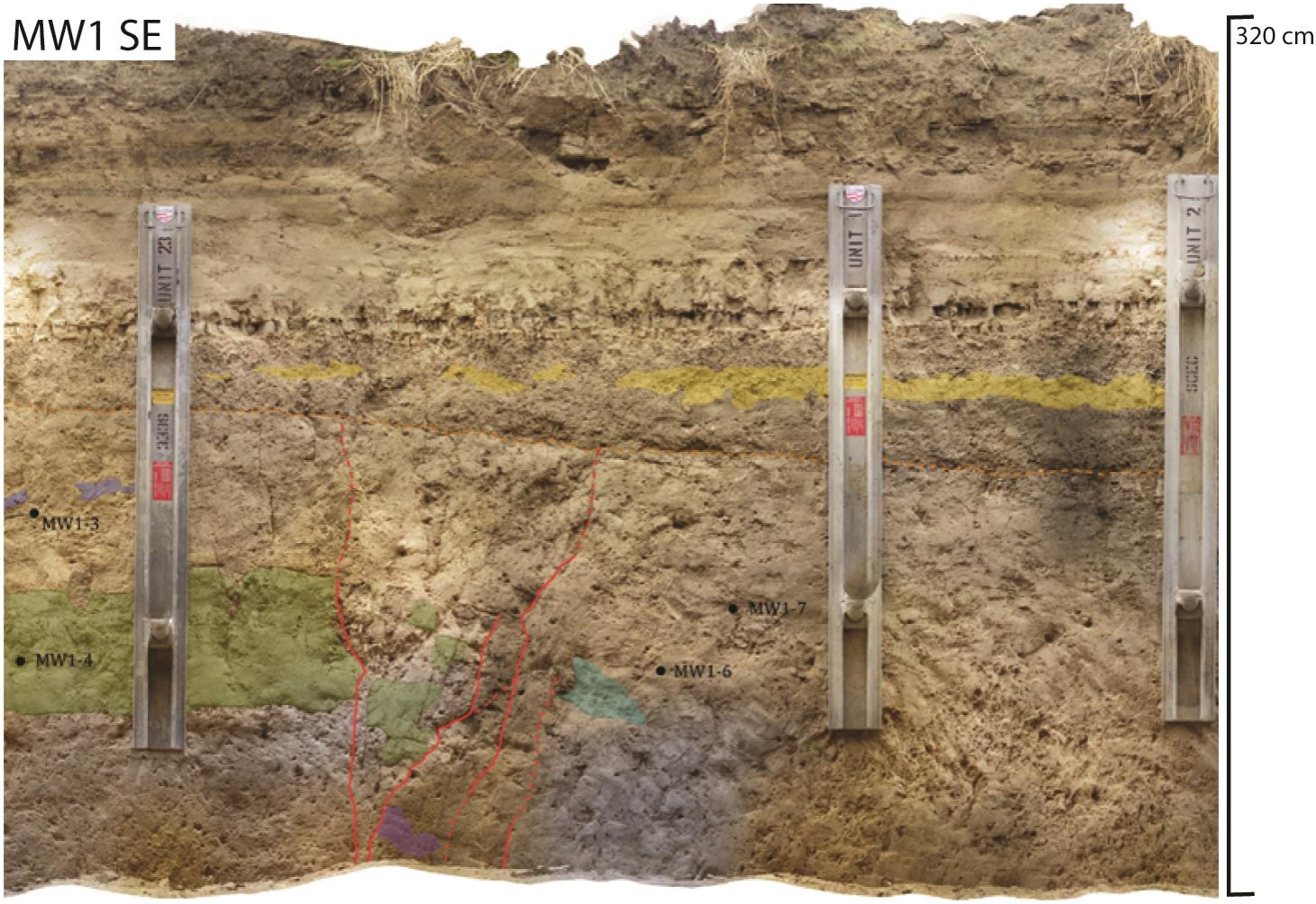

Figure 3. Partial trench log of MW1 SE wall fault zone showing poor stratigraphic preservation and the locations of the radiocarbon samples collected. Red box on Figure 2 SfM indicates the location of this log in the trench. Colors are not related to the stratigraphic column in Figure 4.

Sample Name	Fraction Modern	±	$D^{14}C$ (‰)	±	^{14}C Age (BP)	±
MW1-3	0.7031	0.0014	-296.9	1.4	2830	20
MW1-4	0.6834	0.0014	-316.6	1.4	3060	20
MW1-7	0.8719	0.0017	-128.1	1.7	1100	20
MW1-6	0.8803	0.0026	-119.7	2.6	1025	25

Table 1. Miller's Well radiocarbon ages analyzed in the Keck AMS laboratory at the University of California, Irvine (https://sites.uci.edu/keckams/). Radiocarbon concentrations are given as fractions of the Modern standard, D14C, and conventional radiocarbon age, following the conventions of Stuiver and Polach (Radiocarbon, v. 19, p.355, 1977).

Figure 4. Stratigraphic column of MW3 and MW4 displaying young fan material to at least 3.25 m depth.

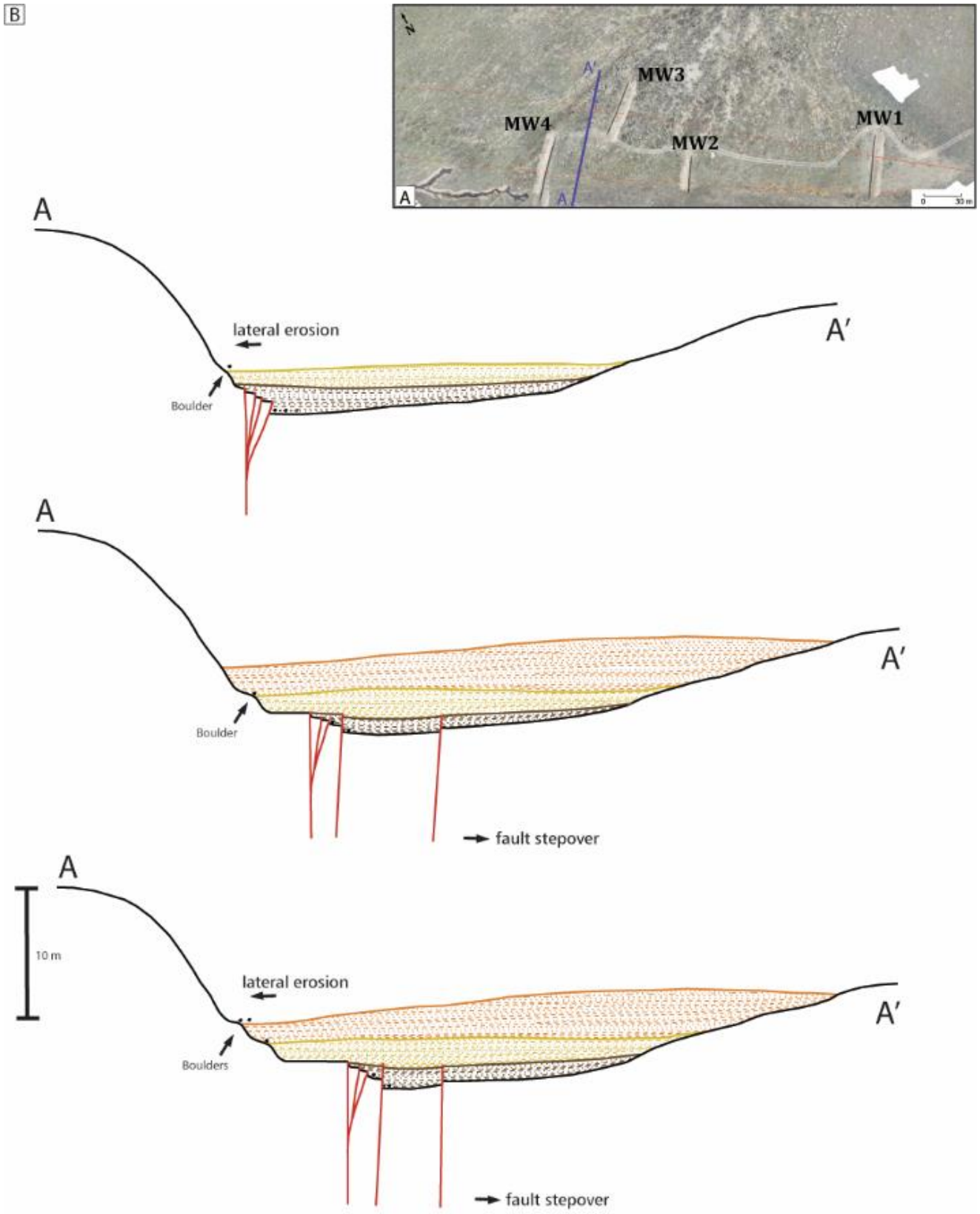

Figure 5. Idealized cross section of the alluvial fan at Miller's Well with vertical exaggeration. A) Orthophoto map of the Miller's Well site in the top right corner indicates the location of cross section as "A" to "A'" in blue. This example focuses on the thickest part of the fan near MW3 and MW4 and projects the fault zone based on the fault trace location in MW1. Color variation in fan deposition represents changes in depositions between periods of major erosion. Black boulders represent much other alluvial fan deposition on top of the shutter ridges that have dropped onto the modern fan and are not sourced from the bedrock.

LY4

Site geomorphology

The LY4 paleoseismic site is located near Las Yeguas Canyon and was previously excavated in1999 (Stone et al., 2002) and 2000 (Young et al., 2002) (Figures 1 and 6). This site is located northeast of linear ridges bounding an early 20th century dammed stock pond that has since been drained. The site has several fans depositing up against the SAF-bounded NE facing scarps and in the small and large wind gaps just southwest and northwest of the trenches (Arrowsmith and Zielke, 2009). The LY4 trenches are located on the alluvial fan that buries the surface expression of the SAF (Figure 6). The geomorphic expression of the fault here is less pronounced than the trace farther southeast or northwest, aiding in fault trace projection (but also the sedimentation rate is well suited for targeting multiple events in the upper several meters of stratigraphy.

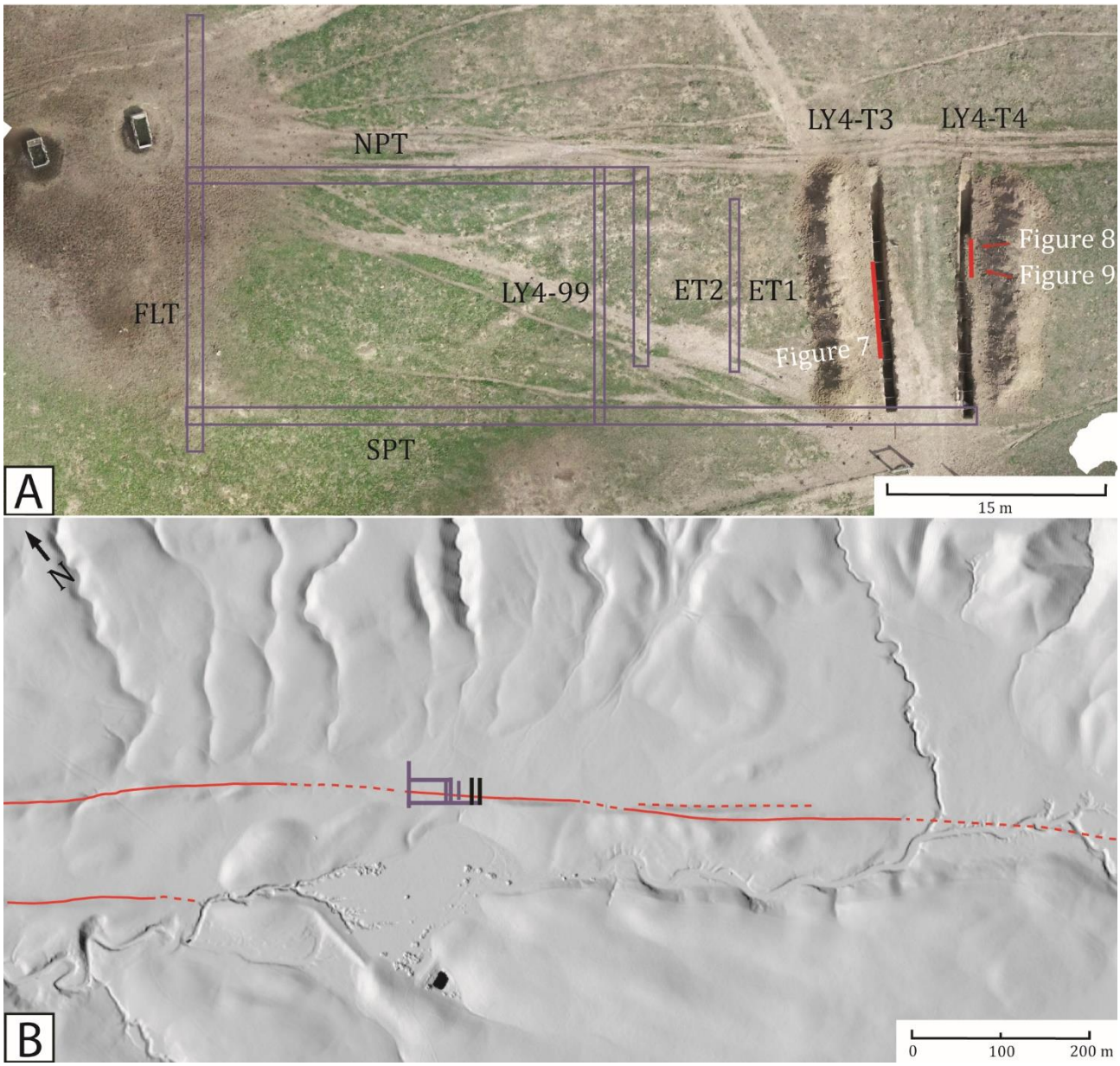

Figure 6. Maps of LY4 Paleoseismic site along SAF Cholame section. B) B4 lidar hillshade showing the location of the LY4 trenches at the bottom. Purple boxes are the previously excavated trenches from Stone et al. (2002) Young et al. (2002), black boxes are the trenches excavated in this project. A) High resolution Structure from Motion orthophoto of the trenches at LY4 derived from UAS aerial photography. Purple polygons are the previously excavated trenches, red lines show the extent of the logs in Figure 7, 8, and 9.

We excavated two new fault perpendicular trenches at the LY4 paleoseismic site just southeast (20 m) of the trenches reported in Stone et al., (2002) and Young et al., (2002) (Figure 6). We have qualitatively rated the observations for at this location using the same scale as the Annette Paleoseismic site, as modeled by Scharer et al., (2017). Each piece of evidence logged has been given a ranking to indicate our confidence that the event horizon is correctly placed. See Table 2 for a generalized list of geomorphic and tectonic indicators, and Table 3 for the full list and rankings for these interpreted earthquakes.

Site excavation

Fault zone stratigraphy consists of alternating finely bedded sand, silt, and gravel strata, and bioturbated soil horizons (buried A horizons which represent paleo-surfaces). There is coarser, well-sorted gravel near the bottom of the trench that fills several small paleochannels. The fault zone is ~4 m wide and is expressed as a graben. Sediments are derived or reworked from the Paso Robles, Monterey, and Temblor Formations. The stratigraphy can be divided into four groups by the presence of the buried A soil horizons. Unit 100, a coarse sand, and overlying strata are interpreted as modern sand and silt deposits that are more continuous and less bioturbated than the sediment packages in the other groups. The section from unit 250 up to the buried A soil horizon underneath Unit 100 comprises the second group, which is characterized by thin, discontinuous fine sand and silt strata. These units are distinctly different from the third group, Unit 380 up to the buried A soil horizon under Unit 250, which contains a well-developed paleo-top soil (Ab horizon) and thick gravel deposits. Group 4 encompasses the soil underneath Unit 380 to the bottom of the trench and contains similar gravels to Group 3 but within a more bioturbated zone that is also more indurated. Our preliminary interpretations correlate Unit 380 with units 16 and 16a and Unit 100 with unit 1b from the earlier trenches ET1 and ET3 (Young et al, 2002). Stratigraphic correlations will be refined and expanded after radiocarbon analysis (currently underway at Keck AMS laboratory at the University of California, Irvine).

Results

There is evidence for up to seven surface ruptures exposed in the new LY4 trenches, of which 5 are good quality (Table 3). The events are numbered such that E1 through E7 have increasing numbers with increasing age and depth. Four of the event horizons have excellent evidence whereas E3, E6, and E7 are less certain. In addition to the overview log shown in figure 7, numerous lines of evidence are presented in the subsequent figures. The locations are designated by boxes in Figure 7.

We infer that E1 is likely the 1857 surface rupture and evidence for this rupture is good quality based on the descriptions in Table 3. It is represented by several fault splays on the western end of the 3m wide fault zone that display small vertical offsets, small channel fills that are offset, sheared blocks, a fissure fill and broken sand blocks that appear to be the remnants of a mole track, affecting Unit 100 through Unit 80. E1 is capped by continuous modern soil in T4 but has no obvious terminus in T3. Units display vertical separations ranging from 50 cm at the base to 3 cm at the modern soil horizon.

Evidence for E2 is present along the western extent of the fault zone. This event has fewer splays than events like E3, E4, E5, however it has higher quality evidence giving it good ranking (Table 3). Main splays terminate in small ~5 cm apparent vertical separation and pop-up features that are capped by continuous strata or broken silt layers with smaller vertical separations (Figure 7).

The principal evidence for E3 is a low angle thrust that disrupts Unit 260 and is capped by flat and continuous Unit 250 in T4. This event is ranked as the lowest quality due to the uncertainty associated with upward termination of splays in E4 (Table 3). Unit 250 in T3 is more disrupted by bioturbation but appears to still cap the splay and discontinuous Unit 260 (Figure 8).

E4 is represented by many splays in both T3 and T4 and breaks stratigraphic units that can be correlated between trenches. It is possible that many of the event indicators attributed to E4 could be attributed to E3 as there is a lack of evidence for upward termination of E4. In some locations, E3 disrupts a continuous silt layer that is ~12 cm thick. Fault splays that ruptured in E4 tend to exhibit a shallow angle with a thrust component and colluvial wedges (Figure 9). The similarity of fault splay angles between the two events could indicate that E4 splays are E3 splays that did not reach the surface. The event evidence Table 3 shows the alternative assignments and sum totals in the two columns on the far right. Discussion at

the trench review highlighted a single splay that broke Unit 160 and was capped by flat and continuous Unit 150, which is broken by other splays attributed to E3. This indicates erosion above Unit 160 and deposition of Unit 150 between E4 and E3. We conclude it is two separate rupturing events due to the lack of constraint on E3 boundaries and the sharpness of the E4 splay that is capped by the silts.

E5 is also characterized by low angle splays with a thrust component but with much larger apparent vertical separations than other events. It is capped by the soil above Unit 320 which it seems to have folded but not broken through (Figure 8). E5 is a good quality event due to the number of event indicators on many splays, rather than the high quality of event indicators as in E2 (Table 3).

E6 is capped by the soil above Unit 370 and has similar thrust components and offset to E5 with an indistinct upward terminus likely due to post event soil development. E6 has both a large number of splays and higher quality event indicators, resulting in the largest total sum in Table 3. Some event indicators for E6 could be attributed to E5 which is reflected in the alternative sum column in Table 3. Field discussion concluded E6 is a separate event because each splay does not appear to disrupt the soil which is flat and gently sloping, without any evidence to indicate a colluvial wedge. Well-developed and bioturbated A horizon soil beneath Unit 320 supports considerable time and erosion occurred between E5 and E6 (Figure 9).

The apparent vertical separation between Units 480 and 500 was double that as observed for between E6 and E5 among all fault splays.E7 may not be well supported by observations, however there was positive feedback at the trench review to suggest that there is a seventh event at this stratigraphic (Table 3).

This site contains abundant detrital charcoal in many of the units and grass burn horizons that provide great potential for bracketing the ages of these paleoearthquakes. COVID-19 has delayed dating plans, but we will be processing 50 samples at the UC Irvine Keck Radiocarbon Facility. We are in the process of correlating stratigraphy with the strata exposed in the earlier trenches by Stone et al. (2002) and Young et al. (2002), which our dates should significantly refine.

-

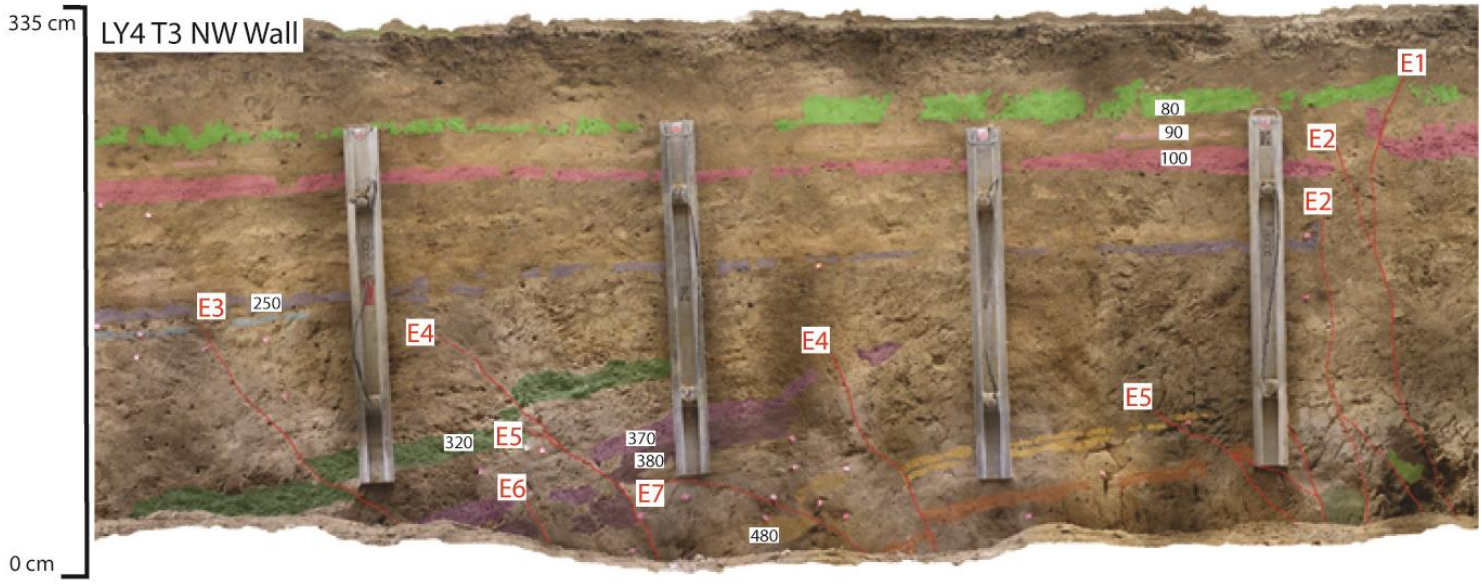

Figure 7. Orthophotos of the LY4 T3 partial NW trench wall created in Agisoft Photoscan and Metashape, overlain by color indicating significant stratigraphic units. Numbers correspond to the Event evidence in Table 3, and the red bounded boxes indicate the event horizon.

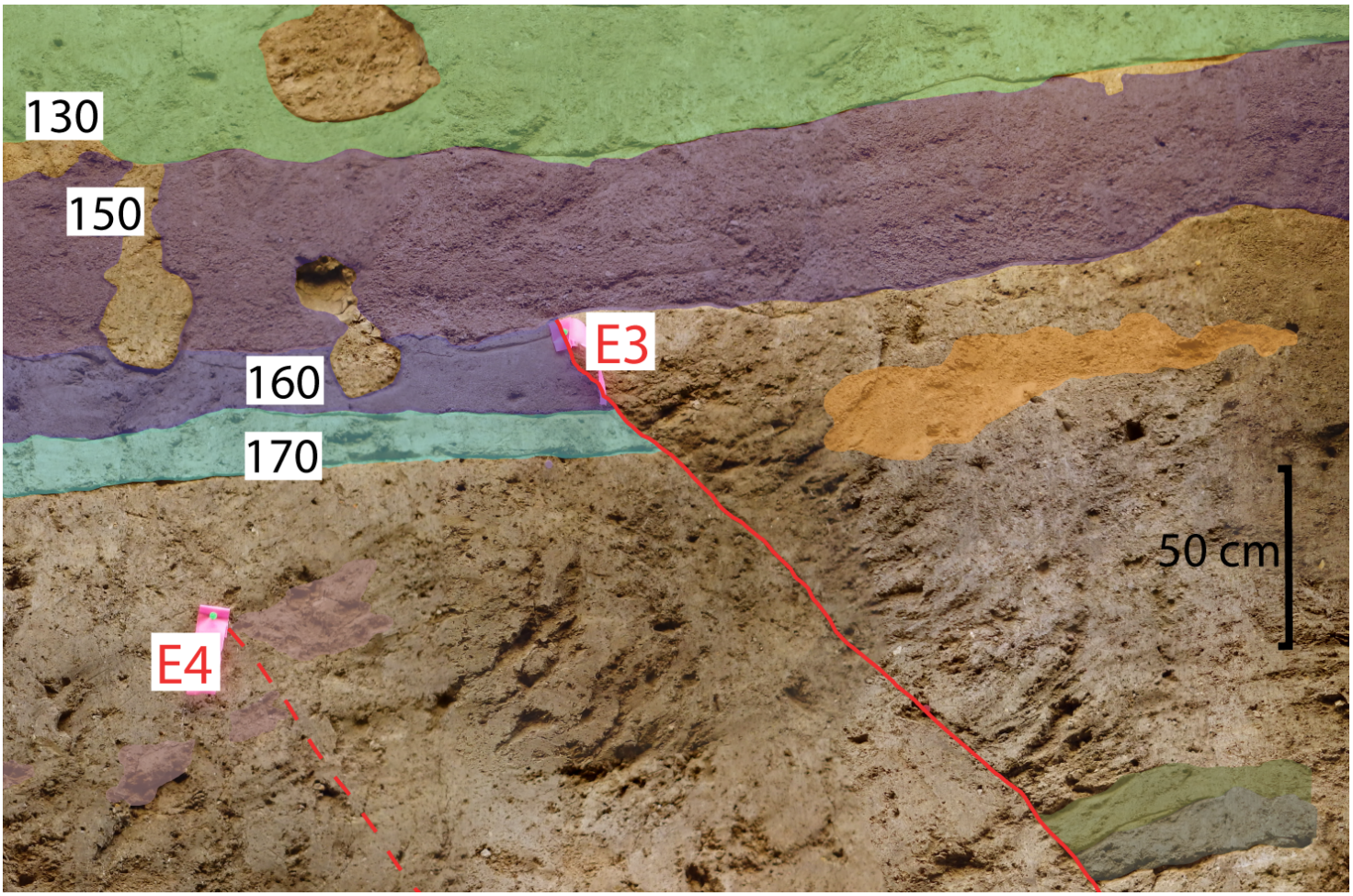

Figure 8. Evidence for E3 and E4. Orthophoto of the LY4 T4 SE trench wall created in Agisoft Photoscan and Metashape, 6 m from the NW end of the trench, overlain by color indicating significant stratigraphic units. Numbers in black correspond to the stratigraphy Event evidence in Table 3, and the red bounded boxes indicate the event horizon.

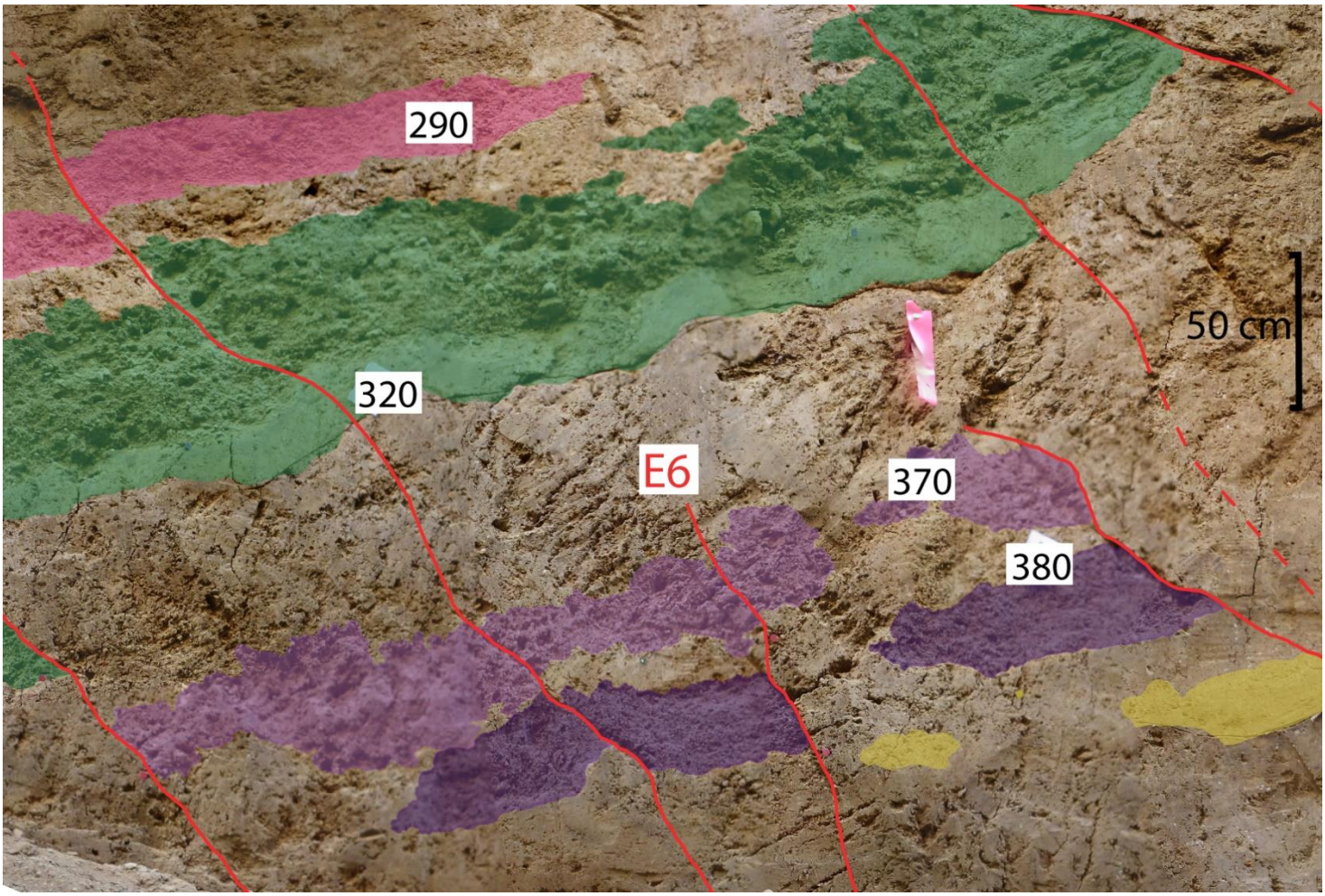

Figure 9. Orthophoto of the LY4 T4 SE trench wall created in Agisoft Photoscan and Metashape, 8 m from the NW end of the trench, overlain by color indicating significant stratigraphic units. Numbers in black correspond to the stratigraphy Event evidence in Table 3, and the red bounded boxes indicate the event horizon.

Quality Rating	Description
0	Fault tip where upper termination is not distinct due to unclear stratigraphy
1	Shear fabric, soil color change, aligned clasts, gradual thickness changes above earthquake horizon, offset stratigraphy or geomorphic features
2	Truncation of units across fault, moderate thickness change above earthquake horizon
3	Fault with apparent vertical offset of units decreasing upsection (AVO-DU), substantial thickness changes but no clearly causative fault
4	Liquefaction, changes in thickness in layers across fault or colluvial wedges, sag deposits, large thickness changes indicative of a rapid filling depression
5	Rotated blocks that are capped by horizontal sedimentation and onlapping sediments, fissures filled by material postdating an inferred event horizon.

Table 2. Quality rating examples and descriptions adapted from Scharer et al. (2017) pertaining particularly to features found in the Annette (Williams, et al., in prep.) and LY4 trenches (this report). Lower numbers indicate lower confidence that the horizon in question was the ground surface at the time of rupture, higher numbers indicate higher confidence.

Event Horizon	Trench Location	Evidence	Quality Ranking	Sum Total	Alternative Event Horizon	Alternative Sum Total
E1	T3-P7-SE	Sheared blocks	1	**29**		**29**
	T3-P7-SE	Thin sand filled fissure leading to a silt pop up (U90)	5			
	T3-P7-SE	Sandy unit broken in moletrack-like uplift (U70)	4			
	T3-P6-NW	U80 pop-up capped by discontinuous sands	3			
	T4-P5-SE	Clay filled cracks cutting U80	3			
	T4-P6-SE	Offset channel	1			
	T4-P6-SE	Truncated silts (U80, U70) capped by continuous silts	4			
	T4-P7-NW	Offset channel	1			
	T4-P7-NW	AVO-DU	3			
	T4-P7-NW	Truncated units past U80 & U70 capped by historic silts	4			
E2	T3-P4-SE	Tilted clay and silt block filling a crack in sand (U150) capped by continuous sand and silts (U100)	4	**25**		**25**
	T3-P6-SE	Pop-up of sands (U180, U150) capped by continuous silts (U90)	4			
	T3-P7-SE	Large fissure fill with broken blocks capped by continuous silts (U90)	5			
	T3-P7-SE	Silt (U90) thickens to the west, possible sag	2			
	T3-P5_shore-NW	Truncated sands and apparent vertical offset capped by U80	4			
	T4-P5-SE	Disrupted units capped by continuous but tilted silts (U80, U70)	3			
	T4-P5-SE	AVO-DU	3			
E3	T3-P4-SE	Apparent vertical offset (U170) capped by flat discontinuous sand (U150)	2	**7**		**21**
	T4-P3-SE	Truncated units (U180, U170) capped by flat sand (U150) **(Figure 8)**	3			
	T4-P4-SE	Decreasing apparent vertical offset (silt)	1			
	T4-P4-SE	Tilted sand unit under continuous sand (U150)	1			

E4	T3-P3-SE	AVO-DU capped by continuous silt (190)	3	**30**	E3	**15/12**
	T3-P4-SE	Shear fabric	1		E3	
	T3-P4-SE	Broken tilted silt and gravel capped by massive unit and continuous sand unit	2		E3	
	T3-P4-SE	AVO-DU (U250, U290 & U370)	3		E3	
	T3-P3-NW	Apparent vertical offset decreasing upsection, capped by U220	3		E3	
	T3-P5-NW	AVO-DU capped by U200	3		E3	
	T4-P3-SE	Low angle fault splay cutting U290 with sheared sands	2			
	T4-P3-SE T4-P4-SE	AVO-DU (U290 & discontinuous sand) AVO-DU (U290, U270))	3 3			
	T4-P3-NW	Apparent vertical offset capped by silt (U160)	4			
	T4-P3-NW	AVO-DU (U290, U270)	3		E5	
E5	T3-P3-SE	AVO-DU (U290)	3	**31**		**52**
	T3-P4-SE	Folded silts topped by tilted continuous gravel (U290)	5			
	T3-P4-SE	Colluvial wedge material onlapping gravel fold (U290), topped by tilted continuous gravel unit	5			
	T3-P3-NW	AVO-DU	3			
	T4-P4-SE	Draped and tilted sands against colluvial wedge (beneath U290)	5			
	T4-P4-NW	Folded gravels (U290) with onlapping sands	5			
	T4-P4-NW	Tilted sand block capped by U270	5			

E6	T3-P4-SE	Offset gravels (U370, U380) capped by thin continuous sand (U320) and soil (U300, U320)	5	**45**		**57/27/39**
	T3-P5-SE	Truncated sands (U380, U390) under discontinuous draped gravel (U370)	4			
	T3-P5-SE	AVO-DU (U390, U380) decreases by half upsection (U370), possible eroded scarp	3			
	T3-P5-NW	Truncated sand units (U400, U390, U380) capped by continuous sand	5			
	T4-P4-SE	Three splays with apparent vertical offset of sands (U380, U370) capped by gravel (U290) and discontinuous sand (U320) **(Figure 9)**	5 x 3		E5	
	T4-P5-SE	AVO-DU	3		E5	
	T4-P5-NW	Offset sands capped by continuous draped gravels (U290, U270)	5			
	T4-P4-NW	Truncated gravel unit	1			
	T4-P4-NW	Fault splay with shear fabric capped by U270	4			
E7	T3-P7-SE	Flat sand block truncated by clay on the west side	2	**12**	E6	0
	T3-P6-NW	Truncated clay	1		E6	
	T4-P6-SE	Offset sands capped by U500 drape	5		E6	
	T4-P6-NW	Offset sand (U480) capped by discontinuous drape (U500)	4		E6	

Table 3. List of geomorphic and tectonic indicators for all event horizons for each fault splay in T3 and T4. The trench column lists the location of each splay on either the NW or SE wall, using the hydraulic shore separation as panel increments, starting on the NE and moving SW. Common event evidence has been abbreviated in the table, e.g. apparent vertical offset decreasing up-section (AVO-DU). Multiplier by the rating indicates multiple splays with the same evidence and are summed together. The numbers are the ratings assigned to each indicator based on Table 2 and Scharer et al. (2017), and the total sums are in the columns in the bolded collumn. For evidence that may have been attributed to a different event horizon, we have listed it as the horizon we have the most confidence in and recorded the alternative in the end columns. The alternative sum scores provide an idea of the change in scoring should those pieces of evidence be subtracted or added to the definite to total sum.

References

Akçiz, S. O., Ludwig, L. G., Arrowsmith, J. R., & Zielke, O. (2010). Century-long average time intervals between earthquake ruptures of the San Andreas fault in the Carrizo Plain, California. *Geology, 38*(9), 787-790.

Bevis M. Hudnut K. Sanchez R. Toth C. Grejner-Brzezinska D. Kendrick E. Caccamise D. Raleigh D. Zhou H. Shan S. Shindle W. Yong A. Harvey J. Borsa A. Ayoub F. Shrestha R. Carter B. Sartori M. Phillips D. Coloma F., 2005, The B4 Project: Scanning the San Andreas and San Jacinto Fault Zones: Eos (Transactions, American Geophysical Union), Fall Meeting 2005, abstract #H34B-01.

Biasi, G. P. (2013). Appendix H: Maximum likelihood recurrence intervals for California paleoseismic sites. *US Geol. Surv. Open-File Rept. 2013-1165-H and Calif. Geol. Surv. Special Rept. 228-H.*

Hilley, G. E., Arrowsmith, J. R., & Amoroso, L. (2001). Interaction between normal faults and fractures and fault scarp morphology. *Geophysical Research Letters, 28*(19), 3777-3780.

Lienkaemper, J. J. (2001). 1857 slip on the San Andreas fault southeast of Cholame, California. *Bulletin of the Seismological Society of America, 91*(6), 1659-1672.

Salisbury, J. B., Arrowsmith, J. R., Rockwell, T, Akciz, S. O., Brown, N., Grant, L. B. (In Prep). The age and origin of small offsets at Van Matre Ranch along the San Andreas Fault in the Carrizo Plain, California.

Scharer, K., R. Weldon, G. Biasi, A. Streig, and T. Fumal (2017), Ground-rupturing earthquakes on the northern Big Bend of the San Andreas Fault, California, 800 A.D. to present, *J. Geophys. Res. Solid Earth, 122*, doi:10.1002/2016JB013606.

Scharer, K., Weldon, R., Streig, A., & Fumal, T. (2014). Paleoearthquakes at Frazier Mountain, California delimit extent and frequency of past San Andreas Fault ruptures along 1857 trace. *Geophysical Research Letters, 41*(13), 4527–4534. https://doi.org/10.1002/2014GL060318

Sieh, K. E., & Jahns, R. H. (1984). Holocene activity of the San Andreas fault at Wallace creek, California. *Geological Society of America Bulletin, 95*(8), 883-896.

Sieh, K. E. (1978). Slip along the San Andreas fault associated with the great 1857 earthquake. *Bulletin of the Seismological Society of America, 68*(5), 1421-1448.

Sieh, K. E. (1978). Prehistoric large earthquakes produced by slip on the San Andreas fault at Pallett Creek, California. *Journal of Geophysical Research: Solid Earth, 83*(B8), 3907-3939.

Stone, E. M., Grant, L. B., & Arrowsmith, J. R. (2002). Recent rupture history of the San Andreas fault southeast of Cholame in the northern Carrizo Plain, California. *Bulletin of the Seismological Society of America, 92*(3), 983-997.

Toké, N. A., & Arrowsmith, J. R. (2006). Reassessment of a slip budget along the Parkfield section of the San Andreas fault. *Bulletin of the Seismological Society of America, 96*(4B), S339-S348.

Williams, A. M., Testing the shorter and variable recurrence interval along the Cholame segment of the San Andreas Fault, Paleoseismology Active Tectonics and Archeoseismology, (2017). In Vol. 8: Proceedings of the 8th International INQUA Meeting on Paleoseismology, Active Tectonics and Archeoseismology (PATA), 23-28 November 2017, Blenheim, New Zealand.

Williams, A. M., Arrowsmith, J R., Rockwell, T.K., Akciz, S. O., and Grant Ludwig, L. (2016). Shorter and variable recurrence intervals along the Cholame segment of the San Andreas Fault; Paleoseismology Active Tectonics and Archeoseismology, 2017. In Vol. 8: Proceedings of the 7th International INQUA Meeting on Paleoseismology, Active Tectonics and Archeoseismology (PATA), 30 May - 2 June 2016, Crestone, Colorado.

Young, J. J., Arrowsmith, J. R., Colini, L., Grant, L. B., & Gootee, B. (2002). Three-dimensional excavation and recent rupture history along the Cholame section of the San Andreas fault. *Bulletin of the Seismological Society of America, 92*(7), 2670-2688.

Zielke, O., Arrowsmith, J. R., Ludwig, L. G., & Akçiz, S. O. (2010). Slip in the 1857 and earlier large earthquakes along the Carrizo Plain, San Andreas fault. *Science, 327*(5969), 1119-1122.

Zielke, O., Arrowsmith, J. R., Ludwig, L. G., & Akciz, S. O. (2012). High-Resolution Topography- Derived Offsets along the 1857 Fort Tejon Earthquake Rupture Trace, San Andreas Fault. *Bulletin of the Seismological Society of America, 102*(3), 1135-11

Project data

Site mapping orthophotography and digital elevation model data from this project will be published on the OpenTopography Community dataspace (https://portal.opentopography.org/dataCatalog?group=dataspace) once processing is complete.

Trench photography and logs will be available from Alana Williams (Alana.M.Williams@asu.edu) or Ramon Arrowsmith (ramon.arrowsmith@asu.edu) in the School of Earth and Space Exploration at Arizona State University. Ultimately these materials will be included in the Ph.D. dissertation of Alana Williams (expected completion second half of 2021).

Bibliography of all publications resulting from the work performed under the award.

Because field work was completed only in early spring 2020, no presentations or other publications of this work have been made.